AIAA JOURNAL
Vol. 36, No. 1, January 1998

Three-Dimensional Piezoelectric Boundary Element Method

L. R. Hill* and T. N. Farris†
Purdue University, West Lafayette, Indiana 47907-1282

The boundary element method is applied to problems of three-dimensional linear piezoelectricity. The continuum equations for conservation of linear momentum and charge are combined into one governing equation for piezoelectricity. A single boundary integral equation is developed from this combined field equation and Green's solution for a piezoelectric medium. Green's function and its derivatives are derived using the radon transform, and the resulting solution is represented by a line integral that is evaluated numerically using standard Gaussian quadrature. The boundary integral equation is discretized using eight-node isoparametric quadratic elements, resulting in a matrix system of equations. The solution of the boundary problem for piezoelectric materials consists of elastic displacements, tractions, electric potentials, and normal charge flux densities. The complete field solutions can be obtained once all boundary values have been determined. The accuracy of this linear piezoelectric boundary element method is illustrated with two numerical examples. The first involves a unit cube of material with an applied mechanical load. The second example consists of a spherical hole in an infinite piezoelectric body loaded by a unit traction on its boundary. Comparisons are made to the analytical solution for the cube and an axisymmetric finite element solution for the spherical hole. The boundary element method is shown to be an accurate solution procedure for general three-dimensional linear piezoelectric material problems.

I. Introduction

THE brothers Pierre and Jacques Curie discovered piezoelectricity in 1880 during their investigation of crystals. A coupling occurs between the electrical and mechanical fields in these materials, such that application of an external mechanical loading induces a change in polarization proportional to it. Conversely, application of an electric field produces a proportional material deformation. This phenomenon was discovered in ceramics in the 1940s, and the subsequent manufactured piezoceramic materials have higher coupling properties than their naturally occurring predecessors. This strong piezoelectric effect has made these materials an important part of the emerging technologies of smart materials and structures. Smart structures are those that incorporate actuators and sensors that are integrated into the structure and have structural functionality. The sensors and actuators are used to influence the structure's states and characteristics. For an extensive review on the applications and advantages of piezoelectric materials and intelligent structures, the reader is referred to the works of Rogers[1] and Crawley.[2]

Analytical solutions to boundary value problems of piezoelectric solids are relatively few in number due to the complexity and anisotropy of the constitutive relations. One segment of research concentrates on inclusions and inhomogeneity problems, including the works of Deeg,[3] Sosa,[4] Pak,[5] Wang,[6] Benveniste,[7] and Chen and Lin.[8] Another line of investigation is concerned with dislocation and crack problems, beginning with Parton[9] and Deeg[3] and continuing more recently with Sosa and Pak,[10] Sosa,[11] Suo et al.,[12] Park and Sun,[13] and Zi-Kun and Shang-Heng.[14] Much of the research focuses on analytical solutions for two-dimensional problems, whereas only a very limited amount of work has been performed on three-dimensional ones.

To consider problems of technical interest, numerical methods must be implemented. Allik and Hughes[15] introduced the finite element method to the solution of piezoelectric vibrations over 25 years ago, and the method's application to general problems of piezoelectricity is possible. Although the finite element method is proven for piezoelectric material analysis, the boundary element method has been shown to have some advantages for three-dimensional problems of flaws and fracture.[16–19] The boundary element method requires only the discretization of the boundary, resulting in a smaller system size than for finite elements. The governing equations are satisfied exactly inside the body, so that relatively coarse meshes produce accurate solutions. In addition, the boundary and finite element methods can be combined in a way that takes advantage of the benefits of each one.

For these reasons, the boundary element method was selected as a means to analyze piezoelectric materials. The pioneering work on boundary elements was performed by Rizzo,[20] Rizzo and Shippy,[21] and Cruse[22] over 20 years ago. Since that time, the method has been applied to many types of problems, including contact mechanics, fracture, voids, and inclusions. Chen and Lin[23] recently developed four-node quadrilateral boundary elements to solve problems of three-dimensional piezoelectric solids. Liu and Farris[24] showed that eight-node quadratic boundary elements were efficient tools for analyzing three-dimensional fracture of isotropic solids. Thus, this paper presents an eight-node piezoelectric boundary element method and illustrates its capabilities with examples.

II. Piezoelectricity Equations

The linear governing equations and constitutive relations for a piezoelectric material in static equilibrium can be expressed as two separate equations, one representing conservation of momentum and the other conservation of electric charge.[25] More information on the piezoelectric standard can be found in Ref. 26. To use these two equations in conjunction with the developed boundary element method, they are combined into one. Barnett and Lothe[27] developed this condensed notation, and Deeg[3] used it in his investigation of piezoelectric dislocations. In these equations, lowercase indices i can have values of 1, 2, or 3, and uppercase indices I can take on values of 1, 2, 3, and 4. The modified governing equation for the piezoelectric material in static equilibrium can be written as[3]

$$\Sigma_{iJ,i} + b_J = 0 \tag{1}$$

where Σ_{iJ} is the stress-electric displacement matrix, defined as

$$\Sigma_{iJ} = \begin{cases} \sigma_{ij} & \text{for} \quad J = 1, 2, 3 \\ D_i & \text{for} \quad J = 4 \end{cases} \tag{2}$$

and b_J is the body load (force and charge) column vector. It is noted that $J = j$ for $J = 1$, 2, or 3. The repeated indices indicate summation in the standard Einstein convention, and the commas indicate differentiation. The combined constitutive relation is written as

$$\Sigma_{iJ} = E_{iJKl} Z_{Kl} \tag{3}$$

Received Oct. 11, 1996; revision received Aug. 4, 1997; accepted for publication Sept. 23, 1997.

*Graduate Research Assistant, School of Aeronautics and Astronautics; currently Senior Member of Technical Staff, Mechanical Analysis Department, TRW Space and Technology Group, One Space Park, R4.2136E, Redondo Beach, CA 90278. Member AIAA.

†Professor, School of Aeronautics and Astronautics. Senior Member AIAA.

where E_{iJKl} is the electroelastic constant matrix

$$E_{iJKl} = \begin{cases} c_{ijkl} & \text{for} \quad J, K = 1, 2, 3 \\ e_{lij} & \text{for} \quad J = 1, 2, 3, \quad K = 4 \\ e_{ikl} & \text{for} \quad J = 4, \quad K = 1, 2, 3 \\ -\varepsilon_{il} & \text{for} \quad J, K = 4 \end{cases} \tag{4}$$

and the strain-electric field matrix Z_{Kl} takes the form

$$Z_{Kl} = \begin{cases} S_{kl} & \text{for} \quad K = 1, 2, 3 \\ \phi_{,l} & \text{for} \quad K = 4 \end{cases} \tag{5}$$

In addition, U_K is the elastic displacement-electricpotential matrix

$$U_K = \begin{cases} u_k & \text{for} \quad K = 1, 2, 3 \\ \phi & \text{for} \quad K = 4 \end{cases} \tag{6}$$

It is of interest to note the symmetries of the elastic, piezoelectric, dielectric, and electroelastic matrices; these can be expressed as, respectively,

$$\begin{gathered} c_{ijkl} = c_{jikl} = c_{jilk} = c_{klij}, \qquad e_{lij} = e_{lji} \\ \varepsilon_{il} = \varepsilon_{li}, \qquad E_{iJKl} = E_{lKJi} \end{gathered} \tag{7}$$

The elastic constants are measured at constant electric potential, the piezoelectric constants are measured either at constant displacement or constant electric potential, and the dielectric constants are measured at constant displacement. In the most general case of an arbitrarily anisotropic (triclinic) material without a center of symmetry, a total of 45 independent material properties are possible, with 21, 18, and 6 values of elastic, piezoelectric, and dielectric constants, respectively. The boundary element method presented in this paper allows for this general case. The examples investigated, however, use the material properties for a typical piezoceramic, which has the symmetry conditions of a hexagonal crystal in class $C_{6v} = 6\,\text{mm}$ (Ref. 25). The total number of independent material properties in this case is 10 because these piezoceramics are elastically transversely isotropic.

The piezoelectric variables Σ_{iJ}, b_J, Z_{Kl}, U_K, and E_{iJKl} are neither tensors nor vectors. They do not obey the appropriate transformation relations in the combined form. To transform from one coordinate system to another, the original field variables, material property matrices, and constitutive relations must be used. Recombination of the variables can occur after the coordinate transform is applied.

III. Boundary Integral Equation

The boundary integral equation is the basis for the numerical implementation of the boundary element method. The development of the boundary integral equation for piezoelectric materials follows a sequence of steps similar to other problem types. This boundary integral equation development is well documented and can be found in many references.[17,28–30] A brief overview of the boundary conditions and necessary equations is presented here.

The piezoelectric boundary integral formulation begins with the static equilibrium equation in three-dimensional space, as combined from Eqs. (1) and (3):

$$(E_{iJKl} Z_{Kl})_{,i} + b_J = 0 \qquad \text{in} \qquad \Omega \tag{8}$$

where Ω is the domain in which the equation holds.

Equation (8) must be solved in reference to boundary conditions. Both mechanical and electrical boundary conditions must be applied for a well-posed piezoelectric boundary value problem. The boundary conditions consist of three types: essential, natural, and mixed. The essential condition is expressed by the displacements and electric potential as

$$u_i = \bar{u}_i \qquad \text{on} \qquad \Gamma^u \tag{9a}$$

$$\phi = \bar{\phi} \qquad \text{on} \qquad \Gamma^\phi \tag{9b}$$

where $\bar{u}_i$ and $\bar{\phi}$ are the known displacements and electric potentials on the boundaries Γ^u and Γ^ϕ, respectively. The natural condition consists of the tractions and normal charge flux densities written as

$$t_i = \bar{t}_i \qquad \text{on} \qquad \Gamma^t \tag{10a}$$

$$q = \bar{q} \qquad \text{on} \qquad \Gamma^q \tag{10b}$$

where $\bar{t}_i = \sigma_{ji} n_j$ and $\bar{q} = \bar{D}_i n_i$ are the known tractions and normal charge flux densities on the boundaries Γ^t and Γ^q, respectively. The mixed condition is a combination of displacements and tractions for mechanical conditions or electric potentials and normal charge flux densities for the electrical conditions, as applied to boundaries $\Gamma^{M_{\text{mech}}}$ and $\Gamma^{M_{\text{elec}}}$, respectively.

For a well-posed boundary value problem, the summation of the boundary segments that have a known boundary condition applied to them must equal the total boundary surrounding the domain of interest, Ω. In particular, this equality must hold for both the mechanical and electrical boundary conditions, respectively, as

$$\Gamma = \Gamma^u + \Gamma^t + \Gamma^{M_{\text{mech}}} \tag{11}$$

$$\Gamma = \Gamma^\phi + \Gamma^q + \Gamma^{M_{\text{elec}}} \tag{12}$$

The piezoelectric boundary integral equation for interior points is defined as

$$\begin{aligned} U_I(p) + \int_\Gamma T^*_{IJ}(p, Q) U_J(Q)\, \mathrm{d}\Gamma &= \int_\Omega U^*_{IJ}(p, Q) b_J(Q)\, \mathrm{d}\Omega \\ &+ \int_\Gamma U^*_{IJ}(p, Q) T_J(Q)\, \mathrm{d}\Gamma \end{aligned} \tag{13}$$

where p is the source point in the domain Ω and Q is the observation point on the boundary Γ. The terms U_J and T_J are the boundary values of elastic displacement/electric potential and traction/normal charge flux density, respectively. The terms U^*_{IJ} and T^*_{IJ} are the influence matrices of the system and are related to Green's function as follows:

$$U^*_{IJ}(\boldsymbol{x} - \boldsymbol{x}') = G_{JI}(\boldsymbol{x} - \boldsymbol{x}') \tag{14}$$

$$T^*_{IJ}(\boldsymbol{x} - \boldsymbol{x}') = E_{kJMn} \frac{\partial G_{MI}(\boldsymbol{x} - \boldsymbol{x}')}{\partial x_n} n_k \tag{15}$$

where $\boldsymbol{x}$ is the observation point, $\boldsymbol{x}'$ is the source point, and n_k is the kth component of the outward unit normal to the surface. Equation (13) is the piezoelectric form of the Somigliana identity and is used to find displacements and electric potentials interior to the boundary once the boundary values U_J and T_J are determined. Using this equation in combination with the constitutive relation, Eq. (3), gives the formulation for the interior stresses and electric displacements.

The source point p is taken to the boundary Γ and represented by P. With both the source and observation points on the boundary, the first integral on the left side of Eq. (13) is singular due to the nature of the fundamental solution. This behavior can be represented by a matrix that is defined by the limit of the singular integral

$$C_{IJ}(P) = \delta_{IJ} + \lim_{\epsilon \to 0} \int_{\Gamma_\epsilon} T^*_{IJ}(P, Q)\, \mathrm{d}\Gamma \tag{16}$$

where Γ_ϵ represents a part of a spherical surface of radius ϵ centered at the load point P on the surface. The remaining integrals in Eq. (13) are determined in the Cauchy principal value sense. Combining this result with Eq. (13) gives the boundary integral equation for piezoelectricity:

$$\begin{aligned} C_{IJ} U_J(P) + \int_\Gamma T^*_{IJ}(P, Q) U_J(Q)\, \mathrm{d}\Gamma \\ = \int_\Omega U^*_{IJ}(P, Q) b_J(Q)\, \mathrm{d}\Omega + \int_\Gamma U^*_{IJ}(P, Q) T_J(Q)\, \mathrm{d}\Gamma \end{aligned} \tag{17}$$

The term C_{IJ} is not evaluated directly but rather is determined using global equilibrium. In addition, the three integrals in Eq. (17) have singularities of the order r^{-2}, r^{-1}, and r^{-1}, respectively. Careful evaluation of these integrals is required as r, the distance between the source and observation points, goes to zero. The numerical discretization of the boundary integral equation is called the boundary element method.

A. Piezoelectric Green's Solution

Green's function for an anisotropic piezoelectric body was derived by Deeg[3] using the radon transform.[31] This solution is written in general form in terms of a surface integral as

$$G_{MR}(\boldsymbol{x}-\boldsymbol{x}') = \frac{1}{8\pi^2 r}\int_{|z|=1}(zz)^{-1}_{MR}\Delta(\boldsymbol{z}\cdot\boldsymbol{\tau})\,\mathrm{d}S(\boldsymbol{z}) \tag{18}$$

where $\boldsymbol{x}'$ is the source point, $\boldsymbol{x}$ is the observation point, and $r = |\boldsymbol{x}-\boldsymbol{x}'|$ is the distance between the two locations. The function $(zz)_{JM}$ is defined as

$$(zz)_{JM} = z_i E_{iJMn} z_n \tag{19}$$

Now consider a coordinate system defined by three mutually orthogonal vectors $\boldsymbol{\tau}-\boldsymbol{m}-\boldsymbol{n}$. Figure 1 depicts this coordinate system in reference to the source and observation points. The spherical angles are defined over the ranges $0 \le \theta \le \pi$ and $0 \le \psi \le 2\pi$. Define a unit vector $\boldsymbol{z}^*$ such that

$$\boldsymbol{z}^* = \boldsymbol{z}[\theta = (\pi/2), \psi] \tag{20}$$

This vector $\boldsymbol{z}^*$ lies in the $\boldsymbol{m}-\boldsymbol{n}$ plane and represents all vectors $\boldsymbol{z}$ that are perpendicular to $\boldsymbol{\tau}$, such that $\boldsymbol{z}^*\cdot\boldsymbol{\tau} = 0$. Equation (18) can then be written in the final simplified form

$$G_{MR}(r\boldsymbol{\tau}) = \frac{1}{8\pi^2 r}\int_0^{2\pi}(z^*z^*)^{-1}_{MR}\,\mathrm{d}\omega \tag{21}$$

where z^* is defined in Eq. (20) and ω is the integration angle, pictured in Fig. 1, with the vector $\hat{m}$ along the line $\omega = 0$. This function can be completely evaluated once a source point, $\boldsymbol{x}'$, and an observation point, $\boldsymbol{x}$, are specified. For each set of points, the values of $\boldsymbol{\tau}$ and r are uniquely determined.

A closer look at Eq. (21) reveals two components of Green's function. The first, represented by $1/r$, is dependent only on the distance between the source and observation points and is singular in nature. The second,

$$\frac{1}{8\pi^2}\int_0^{2\pi}(z^*z^*)^{-1}_{MR}\,\mathrm{d}\omega$$

is dependent on the material properties and the orientation of $\boldsymbol{\tau}$. This line integral contains no singularities and can therefore be evaluated using 20-point standard Gaussian quadrature. A similar conclusion was made by Chen and Lin.[8] The mechanical and electrical behavior of the material can be decoupled by setting the piezoelectric material properties to zero. The mechanical portion of the electroelastic Green's function compares with the closed-form isotropic one for the same elastic material properties. This property was verified numerically.

Two partial derivatives of $G_{MR}(r\boldsymbol{\tau})$ are needed for the boundary element method. The first derivative is used in the boundary integral equation itself, whereas the second derivative is required to determine the interior field stresses and electric displacements. The reader is referred to Ref. 3 for a more complete derivation of the derivatives.

The general form of multiple derivatives of Green's function can be written as

$$\frac{\partial G_{MR}}{\partial x_1\partial x_2\cdots\partial x_n}(\boldsymbol{x}-\boldsymbol{x}') = \frac{1}{8\pi^2|\boldsymbol{x}-\boldsymbol{x}'|^{n+1}}\oint_{|z|=1}\left\{z_1z_2\cdots z_n(zz)^{-1}_{MR}\right\}\delta^{(n)}(\boldsymbol{z}\cdot\boldsymbol{\tau})\,\mathrm{d}S(\boldsymbol{z}) \tag{22}$$

Equation (22) reduces to the following line integral when $\boldsymbol{z} = \boldsymbol{z}^*$:

$$\frac{\partial G_{MR}}{\partial x_1\partial x_2\cdots\partial x_n}(\boldsymbol{x}-\boldsymbol{x}') = \frac{(-1)^n}{8\pi^2|\boldsymbol{x}-\boldsymbol{x}'|^{n+1}}\int_0^{2\pi}\frac{\partial^n}{\partial(\boldsymbol{z}\cdot\boldsymbol{\tau})^n}\left\{z_1z_2\cdots z_n(zz)^{-1}_{MR}\right\}\Big|_{z=z^*}\mathrm{d}\omega \tag{23}$$

in which an apparent typographical error in Ref. 3 has been corrected. Specifically, the first derivative can be expressed as

$$\frac{\partial G_{MR}}{\partial x_i}(r\boldsymbol{\tau}) = \frac{-1}{8\pi^2 r^2}\int_0^{2\pi}\left[\tau_i(z^*z^*)^{-1}_{MR} - z^*_iF^*_{MR}\right]\mathrm{d}\omega \tag{24}$$

where the function F^*_{MR} is defined as

$$F^*_{MR} = (z^*z^*)^{-1}_{MQ}(z^*z^*)^{-1}_{RN}\left[(\tau z^*)_{QN} + (z^*\tau)_{QN}\right] \tag{25}$$

The second derivative is written as

$$\begin{aligned}\frac{\partial G_{MR}}{\partial x_i\partial x_j}(r\boldsymbol{\tau}) = \frac{1}{8\pi^2 r^3}\int_0^{2\pi}\Big\{&2\tau_i\tau_j(z^*z^*)^{-1}_{MR}\\ &- 2z^*_iz^*_j(z^*z^*)^{-1}_{MS}(z^*z^*)^{-1}_{RN}(\tau\tau)_{SN} - 2\left(\tau_iz^*_j + z^*_i\tau_j\right)F^*_{MR}\\ &+ z^*_iz^*_j\left[F^*_{MS}(z^*z^*)^{-1}_{RN} + F^*_{RN}(z^*z^*)^{-1}_{MS}\right]\left[(\tau z^*)_{SN}\right.\\ &\left.+ (z^*\tau)_{SN}\right]\Big\}\,\mathrm{d}\omega\end{aligned} \tag{26}$$

where (τz^*), $(z^*\tau)$, and $(\tau\tau)$ are determined using Eq. (19), replacing the appropriate z.

The derivatives of G_{MR} also consist of a singular part dependent only on the distance between $\boldsymbol{x}'$ and $\boldsymbol{x}$ and a nonsingular part that is orientation dependent. Therefore, the nonsingular line integral here can also be accurately evaluated with Gaussian quadrature, with 20 points providing convergence.

B. Internal Stresses and Electric Displacements

Equation (13) is used in its current form to determine the elastic displacements and electric potentials interior to the boundary once the boundary solution has been completely determined. The internal strains and electric fields are also of interest and are determined by differentiating Eq. (13):

$$\begin{aligned}Z_{kl}(p) = &\int_\Gamma\left\{\frac{1}{2}\left[\frac{\partial U^*_{kM}(p,Q)}{\partial x_l} + \frac{\partial U^*_{lM}(p,Q)}{\partial x_k}\right]\right\}T_M(Q)\,\mathrm{d}\Gamma\\ &- \int_\Gamma\left\{\frac{1}{2}\left[\frac{\partial T^*_{kM}(p,Q)}{\partial x_l} + \frac{\partial T^*_{lM}(p,Q)}{\partial x_k}\right]\right\}U_M(Q)\,\mathrm{d}\Gamma\end{aligned} \tag{27}$$

$$\begin{aligned}Z_{4l}(p) = &\int_\Gamma\left[\frac{\partial U^*_{4M}(p,Q)}{\partial x_l}\right]T_M(Q)\,\mathrm{d}\Gamma\\ &- \int_\Gamma\left[\frac{\partial T^*_{4M}(p,Q)}{\partial x_l}\right]U_M(Q)\,\mathrm{d}\Gamma\end{aligned} \tag{28}$$

The stresses and electric displacements are determined by combining Eq. (27) with the constitutive relation, Eq. (3), to get

$$\Sigma_{iJ}(p) = \int_\Gamma D_{MiJ}(p,Q)T_M(Q)\,\mathrm{d}\Gamma - \int_\Gamma S_{MiJ}(p,Q)U_M(Q)\,\mathrm{d}\Gamma \tag{29}$$

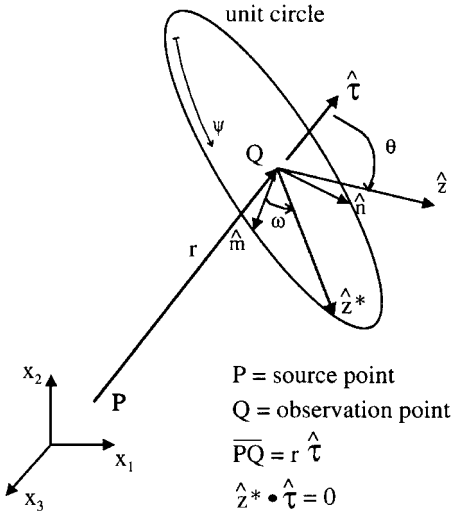

Fig. 1 Variable definition for the derivation of Green's function.

The terms D_{MiJ} and S_{MiJ} are written in terms of the Green's function derivatives, Eqs. (24) and (26), as

$$D_{MiJ} = -E_{iJkl}\frac{1}{2}\left(\frac{\partial G_{Mk}}{\partial x_l} + \frac{\partial G_{Ml}}{\partial x_k}\right) - E_{iJ4l}\frac{\partial G_{M4}}{\partial x_l} \tag{30a}$$

$$\begin{aligned} S_{MiJ} = -E_{iJkl}\frac{1}{2}\Bigg\{\Bigg[E_{rMpq}\frac{1}{2}\left(\frac{\partial G_{pk}}{\partial x_l \partial x_q} + \frac{\partial G_{qk}}{\partial x_l \partial x_p}\right)n_r \\ + E_{rM4q}\frac{\partial G_{4k}}{\partial x_l \partial x_q}n_r\Bigg] + \Bigg[E_{rMpq}\frac{1}{2}\left(\frac{\partial G_{pl}}{\partial x_k \partial x_q} + \frac{\partial G_{ql}}{\partial x_k \partial x_p}\right)n_r \\ + E_{rM4q}\frac{\partial G_{4l}}{\partial x_k \partial x_q}n_r\Bigg]\Bigg\} - E_{iJ4l}\Bigg[E_{rMpq}\frac{1}{2}\left(\frac{\partial G_{p4}}{\partial x_l \partial x_q} \\ + \frac{\partial G_{q4}}{\partial x_l \partial x_p}\right)n_r + E_{rM4q}\frac{\partial G_{44}}{\partial x_l \partial x_q}n_r\Bigg] \end{aligned} \tag{30b}$$

Note that the minus signs in Eqs. (30a) and (30b) come from differentiation with respect to the source point $\boldsymbol{x}'$ rather than the observation point $\boldsymbol{x}$.

The terms S_{MiJ} and D_{MiJ} in Eq. (29) are calculated for the selected source point interior to the body. Because this point is not on the boundary, the integrals in D_{MiJ} and S_{MiJ} are not singular and standard Gaussian quadrature is used to evaluate the surface integrals.

C. Complete Boundary Field Solutions

To calculate the tangential strains, an orthogonal axis system is defined in an element. The vectors tangential to the intrinsic coordinate system in the element are not necessarily orthogonal but can be used to define the necessary coordinate system. See Ref. 29 for a more detailed derivation. The coordinate transform $\beta_{ij} = \hat{e}'_i \cdot \hat{e}_j$ between the local ($\hat{e}'$) and the global ($\hat{e}$) systems can then be determined.

The boundary tractions, displacements, electric potentials, and normal charge flux densities are tensors when not written in the combined piezoelectric form. Therefore, they can be transformed to the local coordinate system as

$$\begin{aligned} t'_i = \sigma'_{ji}n'_j = \beta_{ij}t_j, \qquad Q' = D'_i n'_i = Q \\ u'_i = \beta_{ij}u_j, \qquad \phi' = \phi \end{aligned} \tag{31}$$

The local strains and electric fields can be determined from the local displacements and electric potentials as

$$S'_{ij} = \frac{1}{2}\left(\frac{\partial u'_j}{\partial x'_i} + \frac{\partial u'_i}{\partial x'_j}\right) \tag{32a}$$

$$E'_i = -\frac{\partial \phi'}{\partial x'_i} \tag{32b}$$

Specifically, the boundary solution provides the local stresses σ'_{13}, σ'_{23}, and σ'_{33} and the local electric displacement D'_3 directly. The local strains S'_{11}, S'_{12}, and S'_{22} and the local electric fields E'_1 and E'_2 can also be calculated from the known boundary solution. These combine to provide nine knowns in the local coordinate system.

The uncombined constitutive relations[25] can be written in the local element coordinate system and together relate the six stresses and three electric displacements to the six strains and three electric fields. Using these nine equations and nine known local knowns, the remaining unknown local stresses and electric displacements are determined. The local values of the stresses, strains, electric displacements, and electric fields can be transformed back to the global coordinate system using the following relations:

$$\sigma_{ij} = \beta_{pi}\beta_{qj}\sigma'_{pq} \tag{33a}$$

$$S_{ij} = \beta_{pi}\beta_{qj}S'_{pq} \tag{33b}$$

$$D_i = \beta_{ji}D'_j \tag{33c}$$

$$E_i = \beta_{ji}E'_j \tag{33d}$$

IV. Boundary Element Method

A. Equation Assembly

The general piezoelectric boundary integral equation (17) without the body force term takes the form

$$C_{IJ}U_J(P) + \int_\Gamma T^*_{IJ}(P, Q)U_J(Q)\,d\Gamma = \int_\Gamma U^*_{IJ}(P, Q)T_J(Q)\,d\Gamma \tag{34}$$

In general, the surface integrals in Eq. (34) cannot be evaluated directly and therefore must be approximated numerically. The boundary element method discretizes the surface of the domain Ω into a finite number of elements. Over each element, the variation of the geometry and the variables must be described. This boundary discretization is the only approximation used, as the domain is modeled exactly.

The piezoelectric boundary element program developed herein uses eight-node isoparametric quadratic elements. Experience of both finite and boundary element researchers indicates that this element often is the best compromise between accuracy and efficiency.[29] For this selected element, the geometry and boundary variables are related to the eight nodal quantities by quadratic shape functions as follows:

$$f_I = \sum_{c=1}^{8} N_c(\xi_i, \xi_2)x_I^c \tag{35}$$

where f represents either a directional component x for $I = 1, 2, 3$ or a boundary value U or T for $I = 1, 2, 3, 4$ and c indicates the value at the corresponding nodal point. Let the boundary be discretized into N elements. Substitution for the displacement-voltage U_J and the traction-normal charge flux T_J using Eq. (35) in Eq. (36) yields the discretized boundary element system of equations:

$$\begin{aligned} C_{IJ}(P)U_J(P) + \sum_{n=1}^{N}\sum_{c=1}^{8}\bar{A}^{nc}_{IJ}(P, Q)U_J(Q) \\ = \sum_{n=1}^{N}\sum_{c=1}^{8}B^{nc}_{IJ}(P, Q)T_J(Q) \end{aligned} \tag{36}$$

where $\bar{A}^{nc}_{IJ}$ and B^{nc}_{IJ} are related to Green's function as

$$\bar{A}^{nc}_{IJ} = \int_{-1}^{1}\int_{-1}^{1} T^*_{IJ}(P, Q)N_c(\xi_1, \xi_2)J^{nc}(\xi_1, \xi_2)\,d\xi_1\,d\xi_2 \tag{37a}$$

$$B^{nc}_{IJ} = \int_{-1}^{1}\int_{-1}^{1} U^*_{IJ}(P, Q)N_c(\xi_1, \xi_2)J^{nc}(\xi_1, \xi_2)\,d\xi_1\,d\xi_2 \tag{37b}$$

The term $J^{nc}(\xi_1, \xi_2)$ is the Jacobian of isoparametric transformation from the surface Γ to the intrinsic coordinates ξ_1 and ξ_2 and can be calculated from the determinant of the matrix

$$J^{nc}(\xi_1, \xi_2) = \begin{bmatrix} \hat{e}_1 & \hat{e}_2 & \hat{e}_3 \\ \dfrac{\partial x_1(\xi_1, \xi_2)}{\partial \xi_1} & \dfrac{\partial x_2(\xi_1, \xi_2)}{\partial \xi_1} & \dfrac{\partial x_3(\xi_1, \xi_2)}{\partial \xi_1} \\ \dfrac{\partial x_1(\xi_1, \xi_2)}{\partial \xi_2} & \dfrac{\partial x_2(\xi_1, \xi_2)}{\partial \xi_2} & \dfrac{\partial x_3(\xi_1, \xi_2)}{\partial \xi_2} \end{bmatrix} \tag{38}$$

where $\hat{e}_i$ are the unit base vectors for the global Cartesian system. The Jacobian is equal to the magnitude of the normal vector at each location on the surface, such that components of the normal can be determined from the Jacobian equation.

Taking each node of a modeled problem in turn as the source point P and performing the kernel integrations for each observation point Q, a system of linear algebraic equations is formed and is written as

$$[A][U] = [B][T] \tag{39}$$

where $[A]$ and $[B]$ are formed from the 4×4 submatrices defined in Eqs. (37a) and (37b) and the diagonal portion of $[A]$ (when $P = Q$) is the summation of C_{IJ} and $\bar{A}_{IJ}$.

The unknown boundary values in Eq. (36) are the nodal quantities U^{nc}_J and T^{nc}_J, which are independent of the surface integrals. The integrands in Eq. (36) are combinations of known singular functions. This singularity occurs as the distance between the source point and

the observation point goes to zero in the fundamental solution. Three possibilities exist for the relative locations of source and observation points: P and Q are not on the same element, P and Q are on the same element but not equal, and P and Q are the same point. For the case where P and Q are on different elements, standard Gaussian quadrature provides accurate integration. In the second case, i.e., P and Q are on the same element, a linear mapping of the quadrilateral element to triangular elements[32,33] is used to create more Gaussian points near the singular point. This integration scheme has been used to accurately and efficiently handle the singularity.[34–36] When P and Q are collocated, the triangular mapping is used to calculate B^{nc}_{IJ}, whereas global equilibrium is used to determine $\bar{A}^{nc}_{IJ}$. Becker[29] discusses the handling of these three cases in more detail.

Once the system influence matrices have been assembled, application of the known mechanical and electrical boundary conditions to the system of equations in Eq. (39) results in an equation of the form $[D]\{X\}=\{F\}$. A standard matrix solver is applied to this equation and the unknown boundary values determined.

B. Computer Implementation

The piezoelectric boundary element method program (PBEMP) is the numerical implementation of Eq. (36). After the input of the material properties, boundary element mesh, and boundary conditions (both mechanical and electrical), the influence matrices A and B are assembled. Each node in turn is taken to be the source point P. The observation point Q is assigned by looping over all of the elements in order, using each of the local nodes of the element as this point. For each combination of P and Q for the problem, the 4×4 matrices A_{IJ} and B_{IJ} are determined and subsequently placed in the global system matrices. The surface integrals are evaluated using eight by eight Gaussian points for both the off- and on-element area integrations. The term $[A]$ is assembled as a nodal matrix of size $4N \times 4N$, and $[B]$ is assembled as an element matrix of size $4N \times 4\ (8 \times M)$, where N and M are the total number of nodes and elements, respectively. This effectively ensures that the displacements and voltages are continuous at the element junctions but also allows for the tractions and normal charge flux densities to be different on each element face.

The application of the known boundary conditions will transform the system of equations into the form of $[D]\{X\} = \{F\}$. In applying the known boundary values to the system, each element is considered in turn for mechanical and then electrical boundary conditions. The columns of A and B are arranged such that all of the unknown boundary values are located in the column $\{X\}$, and the matrix $[D]$ is composed of a combination of columns of the influence matrices. The components of the system of equations $[D]$, $\{X\}$, and $\{F\}$ have the dimensions of $4N \times 4N$, $4N$, and $4N$, respectively. The solution of this system of equations is determined using a lower-upper decomposition routine.[37]

Once the complete boundary solution has been determined, the displacements, electric potentials, stresses, and electric displacements for points interior to the boundary can be calculated. Using the internal point of interest as the source point p, the matrices $[A]$ and $[B]$ are assembled as described previously. Substitution of these matrices and the known boundary values $\{U\}$ and $\{T\}$ into Eq. (13) provides the solution for displacement and electric potential. A similar procedure is used with Eq. (29) to find internal stresses and electric displacements. The surface integrals that apppear in Eqs. (30a) and (30b) require 12×12 Gaussian points for accurate evaluation.

PBEMP is currently run on an IBM-compatible personal computer with a 90-MHz Pentium™ processor and 32 MB of RAM. Computation time for the 6-element, 20-node example, to be discussed in the following section, is approximately 2 min. Most of the time is taken to determine the influence matrices, which are functions of the numerically determined fundamental solution. As a comparison, the same problem run with a closed-form fundamental solution would take on the order of tens of seconds to complete on a similar machine.

V. Numerical Examples

A Unit Cube Under Mechanical Loading

This first example is used to verify the boundary element method program for the elastic behavior and the direct piezoelectric effect. A cube of piezoelectric material of dimensions $L \times L \times L$ m^3 is subjected to a uniform displacement, $\bar{u}$ without shear traction, on one side in the x direction, while three sides are attached to rollers. The cube is placed under a zero electric field in the z direction, while the x and y faces have zero normal charge flux density. Figure 2a depicts the geometry and the boundary conditions for this case. The material properties for these examples are those for PZT-4, a manufactured piezoceramic, and can be found in Table 1. These properties hold within a range of electric field and strains, which can be obtained from the piezoceramic manufacturer. A reported electric field range for PZT-4 is $-5 \le E \le 20$ kV/cm, with nonlinear behavior, such as depoling, occurring outside these limits. This problem is modeled using 6 elements and 20 nodes, with each face comprising 1 element. Figure 2b depicts the mesh geometry, with element and node numbers, for this case.

The analytical solution for this problem is readily obtained due to the decoupled nature of the problem. Setting the applied displacement $\bar{u}$ equal to 1 mm and the side length of the cube L to 1 m, the values of the stresses, strains, and electric displacements are

$$\sigma_{xx} = 80.85\ \text{MPa}, \qquad D_z = -1.092 \times 10^{-2}\ \text{C/m}^2$$

$$S_{xx} = 1.0 \times 10^{-2}, \qquad S_{yy} = -3.211 \times 10^{-4}$$

$$S_{zz} = -4.464 \times 10^{-4}$$

All other stresses, strains, and electric displacements are zero.

The results from PBEMP are compared with the analytical solution for both locations on the boundary and points interior to the body. Table 2 contains the boundary tractions and normal charge flux densities for each face of the cube. For each element, a value representative of all eight nodes is presented because each node per element has the same solution in this example. The nodal displacements are found in Table 3. The axial tractions and the electric

Table 1 Material properties for the piezoelectric materials used in the numerical examples

		PZT-4	PZT-6B
Elastic properties, $\times10^{10}$ N/m^2	c_{11}	13.9	16.8
	c_{12}	7.78	6.0
	c_{13}	7.43	6.0
	c_{33}	11.3	16.3
	c_{44}	2.56	2.71
Piezoelectric properties, C/m^2	e_{31}	−6.98	−0.9
	e_{33}	13.84	7.1
	e_{15}	13.44	4.6
Dielectric properties, $\times10^{-9}$ C/V-m	ε_{11}	6.00	3.6
	ε_{33}	5.47	3.4

Table 2 Boundary tractions and normal charge flux densities for the cube under axial mechanical loading

Element	t_x, MPa	q, C/m^2
1	−80.85	0.0
2	0.0	0.0
3	0.0	-1.092×10^{-2}
4	0.0	0.0
5	0.0	1.092×10^{-2}
6	80.85	0.0

Table 3 Nodal displacements of the piezoelectric cube under uniaxial mechanical loading

Node	x, m	y, m	z, m	u_x, mm	u_y, mm	u_z, mm
1	0.0	0.0	0.0	0.0	0.0	0.0
2	0.0	0.0	0.5	0.0	0.0	−0.2232
3	0.0	0.0	1.0	0.0	0.0	−0.4464
7	0.0	1.0	0.0	0.0	−0.3211	0.0
8	0.0	0.5	0.0	0.0	−0.1606	0.0
9	0.5	0.0	0.0	0.5000	0.0	0.0
13	1.0	0.0	0.0	1.0	0.0	0.0

Table 4 Internal displacements, stresses, and electric displacements of the piezoelectric cube under uniaxial mechanical loading

x, m	y, m	z, m	u_x, mm	u_y, mm	u_z, mm	σ_{xx}, MPa	D_z, C/m^2
0.25	0.50	0.50	0.2506	−0.1607	−0.2237	80.81	-1.091×10^{-2}
0.75	0.50	0.50	0.7444	−0.1607	−0.2237	80.85	-1.092×10^{-2}
0.50	0.25	0.50	0.5002	−0.0803	−0.2237	80.47	-1.081×10^{-2}
0.50	0.75	0.50	0.5004	−0.2392	−0.2237	80.77	-1.094×10^{-2}
0.50	0.50	0.25	0.5002	−0.1607	−0.1118	80.81	-1.091×10^{-2}
0.50	0.50	0.75	0.5001	−0.1606	−0.3347	80.85	-1.092×10^{-2}

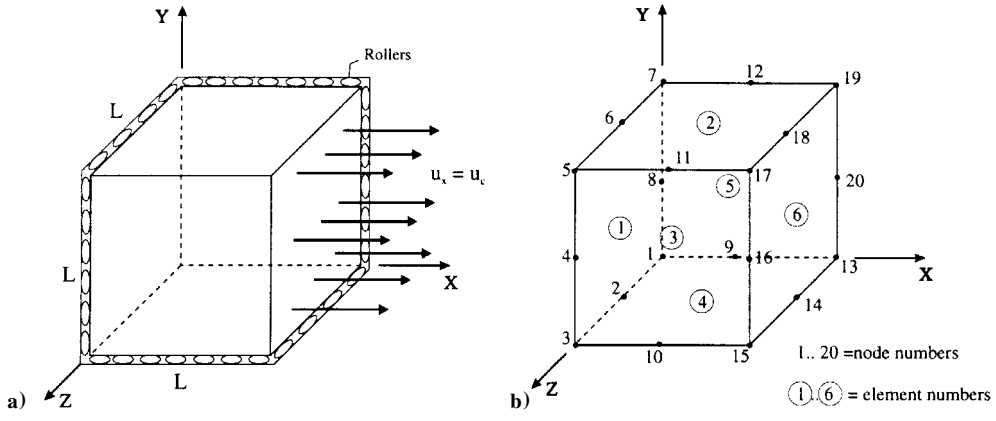

Fig. 2 Cube subjected to a uniaxial mechanical loading condition: a) geometry and applied boundary conditions and b) boundary element mesh, including node and element numbers.

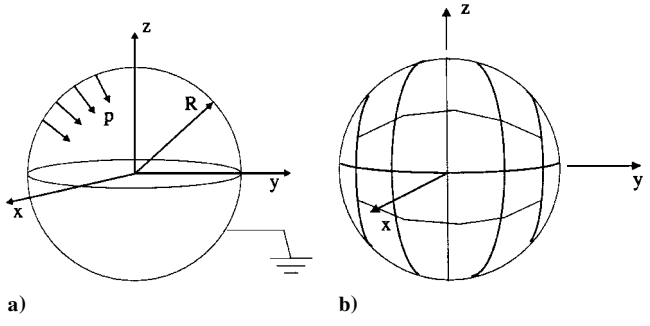

Fig. 3 Hole in the infinite solid: a) geometry and applied boundary conditions and b) boundary element mesh, with identifying node numbers.

displacements are nearly exact when compared with the analytical solution. Solutions interior to the boundary were determined, and Table 4 gives these displacements, stresses, and electric displacements. The electric potential for this example is zero and is not presented. Convergence has been illustrated by solving this problem using 24 total elements, 4 per side of the cube. The same geometry is used with an electrical boundary condition of a constant electric field in the z direction, and similar accuracy is obtained.

B. Spherical Cavity

To further demonstrate the validity of the boundary element method, the more complicated example of a unit spherical cavity inside an infinite body is considered. The boundary of the hole is subjected to a uniform unit internal tension p and a zero normal charge flux density. Figure 3a depicts the geometry and loading conditions. This is a simple problem to model with boundary elements, as the hole itself is the only boundary. A total of 40 elements and 122 nodes were used in the modeling of this spherical surface, as shown in Fig. 3b.

Because the mechanical and electrical parts of the piezoelectric Green's function can be decoupled and the exact solution for this problem exists,[38] PBEMP is first applied to the spherical void example using isotropic material properties. The numerical results of PBEMP are compared with the analytical solution, and the error in

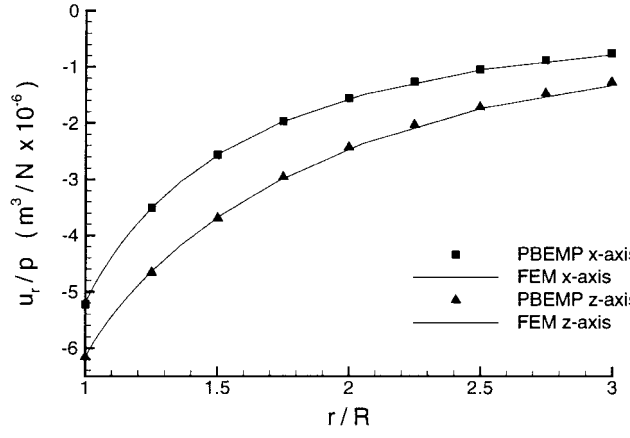

Fig. 4 Radial displacement u_r along the x and z axes.

the radial displacement on the hole boundary is less than 1% for this mesh. Stresses and displacements for points interior to the body are also in good agreement with the exact solution.

The case of a piezoelectric medium is now considered. The material properties for this example are for another member of the PZT family of piezoceramics, PZT-6B. The values of these material properties are found in Table 1. The finite element method is used to determine a comparison solution. The commercial finite element package ABAQUS was used to generate an axisymmetric model of this problem, consisting of 1800 elements. The outer radius used to simulate the infinite space was 10 times the hole radius R. Figure 4 shows the comparison of the boundary element and finite element solutions for the radial displacements along both the x axis and the z axis. Figure 5 presents the stresses σ_{rr}, $\sigma_{\theta\theta}$, and $\sigma_{\phi\phi}$ along the x axis, and Fig. 6 depicts the electric field along the z axis. The boundary element solutions are in good agreement with the finite element results for both points on and interior to the boundary. It is noted that the boundary element model is fully three dimensional, allowing the application of arbitrary loads. The new finite element mesh would require accurate meshing of the complete three-dimensional domain.

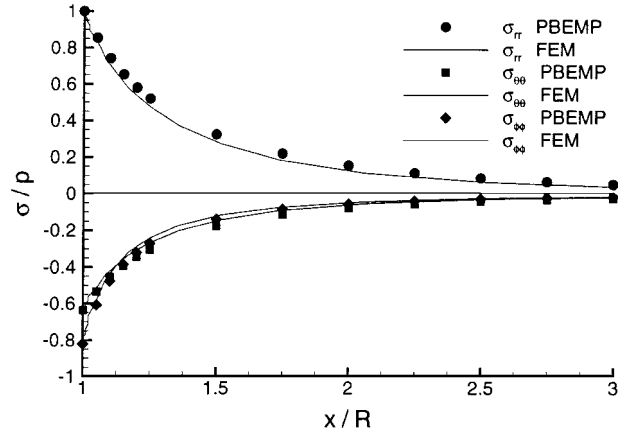

Fig. 5 Stresses σ_{rr}, $\sigma_{\theta\theta}$, and $\sigma_{\phi\phi}$ along the x axis.

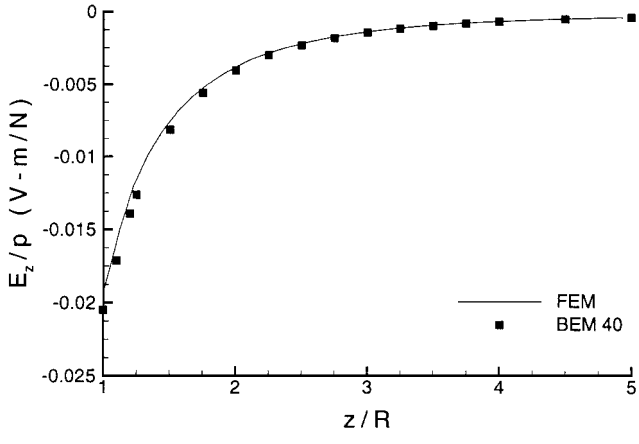

Fig. 6 Electric field E_z along the z axis.

VI. Conclusion

A three-dimensional linear piezoelectric boundary element program has been written and verified. The program can be used to accurately model localized fields resulting from holes and notches in smart structures. Future work includes calculation of strain energy release rates for cracks in piezoelectric media.

Acknowledgment

This research is supported in part by the National Science Foundation under Grant EEC-9402533 to the Engineering Research Center for Collaborative Manufacturing.

References

[1]Rogers, C., "Intelligent Material Systems—The Dawn of a New Material Age," *Journal of Intelligent Materials in Systems and Structures*, Vol. 4, No. 1, 1993, pp. 4–12.

[2]Crawley, E. F., "Intelligent Structures for Aerospace: A Technology Overview and Assessment," *AIAA Journal*, Vol. 32, No. 8, 1994, pp. 1689–1699.

[3]Deeg, W. F., "The Analysis of Dislocation, Crack, and Inclusion Problems in Piezoelectric Solids," Ph.D. Thesis, Stanford Univ., Stanford, CA, May 1980.

[4]Sosa, H. A., "Plane Problems in Piezoelectric Media with Defects," *International Journal of Solids and Structures*, Vol. 28, No. 4, 1991, pp. 491–505.

[5]Pak, Y. E., "Linear Electro-Elastic Fracture Mechanics of Piezoelectric Materials," *International Journal of Fracture*, Vol. 54, No. 19, 1992, pp. 79–100.

[6]Wang, B., "Three-Dimensional Analysis of an Ellipsoidal Inclusion in a Piezoelectric Material," *International Journal of Solids and Structures*, Vol. 29, No. 3, 1992, pp. 293–308.

[7]Benveniste, Y., "On the Micromechanics of Fibrous Piezoelectric Composites," *Mechanics of Materials*, Vol. 18, No. 3, 1994, pp. 183–193.

[8]Chen, T., and Lin, F. Z., "Numerical Evaluation of Derivatives of the Anisotropic Piezoelectric Green's Functions," *Mechanics Research Communications*, Vol. 20, No. 6, 1993, pp. 501–506.

[9]Parton, V. L., "Fracture Mechanics of Piezoelectric Materials," *Acta Astronautica*, Vol. 3, No. 9–10, 1976, pp. 671–683.

[10]Sosa, H. A., and Pak, Y. E., "Three-Dimensional Eigenfunction Analysis of a Crack in a Piezoelectric Material," *International Journal of Solids and Structures*, Vol. 26, No. 1, 1990, pp. 1–15.

[11]Sosa, H. A., "On the Fracture Mechanics of Piezoelectric Solids," *International Journal of Solids and Structures*, Vol. 28, No. 4, 1992, pp. 2613–2622.

[12]Suo, Z., Kuo, C. M., Barnett, D. M., and Willis, J. R., "Fracture Mechanics for Piezoelectric Ceramics," *Journal of the Mechanics and Physics of Solids*, Vol. 40, No. 4, 1992, pp. 739–765.

[13]Park, S. B., and Sun, C. T., "Fracture Criteria for Piezoelectric Ceramics," *Journal of the American Ceramic Society*, Vol. 78, No. 6, 1995, pp. 1475–1480.

[14]Zi-Kun, W., and Shang-Heng, H., "Fields Near Elliptical Crack Tip in Piezoelectric Ceramics," *Engineering Fracture Mechanics*, Vol. 51, No. 3, 1995, pp. 447–456.

[15]Allik, H., and Hughes, T. J. R., "Finite Element Method for Piezoelectric Vibrations," *International Journal for Numerical Methods in Engineering*, Vol. 2, 1970, pp. 151–157.

[16]Mukherjee, S., *Boundary Element Methods in Creep and Fracture*, Elsevier Applied Science, London, 1982.

[17]Beskos, D. E., *Boundary Element Methods in Mechanics*, Elsevier Applied Science, London, 1987.

[18]Cruse, T. A., *Boundary Element Analysis in Computational Fracture Mechanics*, Kluwer Academic, Norwell, MA, 1988.

[19]Banerjee, P. K., and Butterfield, R., *Boundary Element Methods in Engineering Science*, 2nd ed., McGraw–Hill, London, 1981.

[20]Rizzo, F. J., "An Integral Equation Approach to Boundary Value Problems of Classical Elasticity," *Quarterly of Applied Mathematics*, Vol. 25, 1967, pp. 83–95.

[21]Rizzo, F. J., and Shippy, D. J., "A Formulation and Solution Procedure for the General Non-Homogeneous Elastic Inclusion Problem," *International Journal of Solids and Structures*, Vol. 4, 1968, pp. 1161–1167.

[22]Cruse, T. A., "Numerical Solutions in Three Dimensional Elastostatics," *International Journal of Solids and Structures*, Vol. 5, 1969, pp. 1259–1274.

[23]Chen, T., and Lin, F. Z., "Boundary Integral Formulations for Three-Dimensional Anisotropic Piezoelectric Solids," *Computational Mechanics*, Vol. 15, No. 6, 1995, pp. 485–496.

[24]Liu, M., and Farris, T. N., "Boundary Element Crack Closure Calculation of Three-Dimensional Stress Intensity Factors," *International Journal of Fracture*, Vol. 60, No. 1, 1993, pp. 33–47.

[25]Tiersten, H. F., *Linear Piezoelectric Plate Vibrations*, Plenum, New York, 1969.

[26]"IEEE Standards on Piezoelectricity," *IEEE Transactions on Sonics and Ultrasonics*, Vol. 31, No. 2, 1984.

[27]Barnett, D. M., and Lothe, J., "Synthesis of the Sextic and Integral Formalism for Dislocations, Green's Functions, and Surface Waves in Anisotropic Elastic Solids," *Physica Norvegica*, Vol. 7, No. 1, 1975, pp. 12–22.

[28]Brebbia, C. A., and Dominguez, J., *Boundary Elements: An Introductory Course*, 1st ed., Computational Mechanics Publications, Southampton, England, UK, 1988.

[29]Becker, A. A., *The Boundary Element Method in Engineering*, McGraw–Hill, New York, 1992.

[30]Banerjee, P. K., *The Boundary Element Method in Engineering*, 2nd ed., McGraw–Hill, London, 1994.

[31]Gel'fand, I. M., Graev, M. I., and Vilenkin, N. Y., *Generalized Functions*, Vol. 5, Academic, New York, 1966.

[32]Watson, J. O., "Advanced Implementation of the Boundary Element Method for Two- and Three-Dimensional Elastostatics," *Developments in Boundary Element Methods*, edited by P. Banerjee and R. Butterfield, Elsevier Applied Science, London, 1979, pp. 31–63.

[33]Tan, C. L., "Three Dimensional Boundary Integral Equation Analysis of Cracked Components," Ph.D. Thesis, Imperial College, Univ. of London, London, 1979.

[34]Atluri, S. N., "Higher-Order, Special and Singular Finite Elements," *Survey of Finite Element Methods*, edited by A. Noor and W. Pilkey, American Society of Mechanical Engineers, New York, 1980.

[35]Li, H. B., Han, G. M., and Mang, H. A., "A New Method for Evaluating Singular Integrals in Stress Analysis of Solids by the Direct Boundary Element Method," *International Journal for Numerical Methods in Engineering*, Vol. 21, 1985, pp. 2071–2098.

[36]Liu, M., and Farris, T. N., "Three-Dimensional Infinite Boundary Elements for Contact Problems," *International Journal for Numerical Methods in Engineering*, Vol. 36, No. 19, 1993, pp. 3381–3398.

[37]Press, W., Flannery, B., Teukolsky, S., and Vetterling, W., *Numerical Recipes: The Art of Scientific Computing*, Cambridge Univ. Press, Cambridge, England, UK, 1986, Chap. 2.

[38]Timoshenko, S. P., and Goodier, J. N., *Theory of Elasticity*, 3rd ed., McGraw–Hill, New York, 1970, pp. 392–395.

R. K. Kapania
Associate Editor